Low Temperature Performance and Durability of Solid Oxide Fuel Cells with Titanate Based Fuel Electrodes Using Reformate Fuel

Christensen, J. O.; Sudireddy, B. R.; Hagen, A.

Published in:
Journal of The Electrochemical Society

Link to article, DOI:
10.1149/1945-7111/acbb31

Publication date:
2023

Document Version
Publisher's PDF, also known as Version of record

Journal of The Electrochemical Society, 2023 **170** 024515

Low Temperature Performance and Durability of Solid Oxide Fuel Cells with Titanate Based Fuel Electrodes Using Reformate Fuel

J. O. Christensen,[z] B. R. Sudireddy, and A. Hagen

Department of Energy Conversion and Storage, Technical University of Denmark, 2800 Kgs. Lyngby, Denmark

The Ni/YSZ composite electrode is conventionally used for solid oxide cells, in electrolysis (SOEC) as well as fuel cell (SOFC) operation. For enhanced electrochemical performance at low temperature, mechanical durability, and impurity tolerance, alternative fuel electrode materials and cell configurations are required. In this paper we have studied a metal supported cell (MSC) with a titanate based fuel electrode ($La_{0.4}Sr_{0.4}Fe_{0.03}Ni_{0.03}Ti_{0.94}O_3$, LSFNT) for its fuel cell performance using carbon containing fuel and compared to a state of the art (SoA) fuel electrode supported cell with a Ni/YSZ fuel electrode. In hydrogen fuel, the cells showed similar performance at intermediate and low temperatures (750 °C to 650 °C), although the ASR is slightly higher for the MSC at all temperatures and steam/hydrogen ratios. Additionally, the MSC showed fair initial performance in reformate type fuel compositions (CO/steam and CO/steam/hydrogen), i.e. the fuel electrode possesses activity for the water gas shift reaction, which opens the possibility to use such cells with hydrocarbon fuels after a pre-reformer. Durability testing in pre-reformed fuel gas revealed that further fuel electrode tailoring is required to minimize cell degradation in carbon containing fuels.
 [DOI: 10.1149/1945-7111/acbb31]

Manuscript submitted September 20, 2022; revised manuscript received December 11, 2022. Published February 24, 2023.

The fuel flexibility of solid oxide fuel cells (SOFCs) opens for the use of both hydrogen and hydrocarbon fuels. Hydrocarbon fuels are of particular interest for mobile, but also stationary applications, taking advantage of their high energy density. Furthermore, they allow for integration into the present energy infrastructure, where hydrogen is not always available, using e.g. natural gas or biogas.[1,2]

SOFC technology has already reached early commercial levels using state of the art (SoA) cells with Ni/YSZ (Y-stabilized ZrO_2) fuel electrodes operating in hydrocarbon fuel, including stationary and mobile applications.[3–5] However, operation in hydrocarbon fuels bears the risk of degradation due to C deposition, facilitated by the catalytic activity of Ni in the SoA Ni/YSZ composite fuel electrode[6] and sulphur poisoning caused by the trace amounts of sulphur in e.g. natural gas.[7,8] Thus, replacement of the SoA fuel electrode with one that is more tolerant towards carbon deposition and sulphur poisoning is highly desirable. Alternatives include the use of all-ceramic Ni free anodes or anodes with small Ni contents. Interesting candidates include modified oxide perovskites (ABO_3), which have received a lot of attention due to their chemical stability and high electrical conductivity.[9–11] Among these, doped strontium titanates with substitution of catalytically active transition metals on the B-site are interesting for SOFC applications, due to exsolution on the perovskite surface under reducing conditions.[12–14]

In addition to fuel electrode stability and performance, cost-effective cell designs are desirable. The key is lowering operating temperatures to e.g. 650 °C and below, which opens for use of cheaper balance of plant component materials, including metals. Hence, metal supported (MS) SOFCs based on stainless steel supports are receiving increased attention.[15–17] MS-SOFCs combine an increased thermal conductivity, ductility, and resistance to mechanical stresses, which is important e.g. in case of vibrations during mobile applications, with low-cost materials compared to SoA devices based on ceramic and cermet supports, while retaining the fuel flexibility of SOFCs.[18–20] Integration of the Ni/YSZ cermet fuel electrode into MSCs suffers severe processing challenges, due to agglomeration and coarsening of Ni particles during sintering, and interdiffusion of Ni into the steel support.[21,22]

In contrast, doped perovskite fuel electrodes, can be readily integrated into MSCs using conventional tape casting[23,24] Nielsen, et al. reported electrochemical tests of MSCs, fabricated by tape casting, with three different fuel electrode compositions, all including the doped $SrTiO_3$ $La_{0.4}Sr_{0.4}Fe_{0.03}Ni_{0.03}Ti_{0.94}O_3$ (LSFNT), where exsolution of electrocatalytically active Fe and Ni is possible. The electrode backbones were infiltrated with Ni:$Ce_{0.8}Gd_{0.2}O_{1.9}$ (CGO) to further enhance the catalytic activity;[25] A: 95% LSFNT/5% ScYSZ (Sc/Y-stabilized ZrO_2), B: 55% LSFNT/40% FeCr/5% ScYSZ, and C: (20% LSFNT/60% FeCr/20% ScYSZ). The authors recorded polarization curves and impedance data in hydrogen fuel (with 4% and 20% steam) at 750 °C, 700 °C, and 650 °C. Further tests, including durability assessment, in methane/steam revealed much lower open circuit voltage (OCV) values on those MSCs than expected.[24] These lower values as compared to the expected equilibrium gas composition were assigned to the low Ni content in the fuel electrodes of the MSCs, causing insufficient methane reforming activity. The activity of the infiltrated LSFNT fuel electrodes for the water gas shift (WGS) reaction using reformate, CO containing fuel gas has not yet been studied. A sufficient activity for the WGS reaction opens the opportunity to use hydrocarbon fuels after a pre-reforming step prior to the SOFC.

In the current work, a MSC with pure ceramic anode (95% LSFNT/5% ScYSZ, Ni:CGO infiltrated) is investigated and compared to a SoA Ni/YSZ based cell, regarding cell performance in hydrogen and CO containing fuel at temperatures down to 650 °C. Furthermore, cell durability was tested using pre-reformed methane fuel gas mixture (for the MSC) and 20% steam/hydrogen (for Ni/YSZ) at 650 °C. The performance was investigated by polarization curves and electrochemical impedance spectroscopy (EIS).

Experimental

Cell fabrication.—The cells were manufactured at DTU Energy, following conventional ceramic processing techniques such as tape casting and screen printing.

MSCs. The metal supported cell was fabricated according to a previously developed procedure at DTU.[25] The metal support (stainless steel, Fe22Cr, ca. 300 μm), anode backbone ($La_{0.4}Sr_{0.4}Fe_{0.03}Ni_{0.03}Ti_{0.94}O_3$, LSFNT, with 5 vol% ScYSZ, ca. 15 μm), and electrolyte (ScYSZ, ca. 10 μm) layers were fabricated using tape casting. These layers were laminated and co-sintered above 1100 °C in reducing atmosphere (H_2/Ar) to fabricate the half cell, using a proprietary protocol. The half cell was infiltrated with Ni:CGO electrocatalyst - details on the infiltration procedure are described elsewhere.[26] A 1 μm thick $Ce_{0.9}Gd_{0.1}O_{1.95}$ (CGO10) cathode barrier layer to prevent interdiffusion was subsequently deposited with physical vapor deposition (PVD). Finally, a ca. 15 μm thick $(La_{0.6}Sr_{0.4})_{0.99}CoO_{3-\delta}$ (LSC) cathode was applied by screen printing as described in earlier studies and sintered below 1100 °C.[25,27]

[z]E-mail: jeoch@dtu.dk

SoA cell. The anode supported Ni/YSZ cell was manufactured following a known procedure.[28] The support, active fuel electrode, and electrolyte were manufactured by tape casting and sintered together in air above 1200 °C, yielding a half cell with a 300 μm thick Ni/YSZ support layer, a 12–16 μm thick Ni/YSZ active fuel electrode layer, and a ca. 10 μm thick YSZ electrolyte. 8YSZ was used for the electrolyte and active electrode and 3YSZ was used for the Ni/YSZ support. Subsequently, a 6–7 μm thick CGO barrier layer and a ca. 30 μm thick LSC/CGO oxygen electrode were screen printed and sintered below 1100 °C to obtain a full cell.[29]

Electrochemical characterization.—Both cells had a 54 × 54 mm cell area with an active area of 16 cm^2, defined by the screen printed cathode layer. The cells were tested in an alumina housing, usable for both the MSC and the SoA cell.[24] The test protocols for both cells are illustrated in Fig. 1. Ni and Au meshes were used as contact and current collector layers on the anode and cathode side, respectively. The cells were sealed with a gold frame at their edges on the anode side. No sealing was used on the cathode side since the gas was distributed from the middle of the cathode and outwards via milled gas trenches in the alumina top block. After mounting, a weight of 4 kg was applied for sealing and contact reasons, and the cells were heated and tested under the conditions described in Table I. The startup procedure was tailored according to the cell type, i.e. the cell with the Ni/YSZ fuel electrode was treated in hydrogen to the anode to reduce NiO to Ni. On the other hand, the startup of the MSC included in-situ sintering of the cathode (Table I).

The OCV values at the initial, highest temperature in 4% steam/hydrogen, in which the measured values are very sensitive to any gas leaks, were within 15 mV difference to the theoretical values calculated using the Nernst equation, verifying that the cells behaved as expected and no/minor leaks were present in the setup. IV curves and electrochemical impedance spectra were recorded at a standardized set of conditions, called fingerprint, as described in Table I. For iV curves, a lower voltage limit of 600 mV and an upper current limit of 0.63 A cm^{-2} were used to avoid damage to the cells. After the fingerprint, the cells were tested for durability at 650 °C in the gas mixtures described in the introduction section, followed by a final fingerprint.

Results and Discussion

Initial performances in hydrogen fuel.—The initial performances of the cells were tested in hydrogen/steam (4, 20, and for the Ni/YSZ cell also 50% steam) and in CO/steam fuel, simulating a reformate mixture. Fingerprint characterization in high steam content (50% steam/hydrogen) was omitted for the MSC to avoid possible corrosion of the steel support, which has been observed in earlier studies on MSCs.[11] The Ni/YSZ cell was also tested in methane/steam (1:2 ratio). Figure 2 shows iV curves of both cells in steam/hydrogen fuel at varying temperatures and steam to hydrogen ratios. The corresponding area specific resistances (ASRs), determined as the local slope at a current density of 0.25 ± 0.025 A cm^{-2}, are shown in Table II together with the corresponding cell voltages and power densities. In hydrogen/steam fuel, the Ni/YSZ cell has slightly smaller ASR than the MSC at 750 °C and 700 °C. The difference in ASR is larger at 650 °C, although the power density remains similar for the two cells. The power density for both cells decreases at lower temperature and with increasing steam/hydrogen ratio in the fuel.

The higher activity (i.e. lower ASR, higher power density) of the Ni/YSZ at lower operating temperatures is surprising considering the more active oxygen electrode used in the MSC (pure LSC sintered in-situ, yielding smaller structures). Additionally, the fuel electrode in the MSC is infiltrated with mixed ionic/electronic conducting CGO (and Ni), which is absent in the Ni/YSZ composite anode. However, the difference in electrolyte composition/thickness and possible difference in electrolyte/anode current constriction resistance could explain why the MSC did not perform better.

Initial performances in hydrocarbon fuels:.—Steam reforming of hydrocarbons such as methane can occur in steam/methane fuel mixtures on the fuel electrode, which acts as a heterogeneous catalyst in case of Ni/YSZ anodes (Eq. 1). The formed hydrogen (and carbon monoxide) are converted in the electrochemical process. Additionally, carbon monoxide can react through the WGS reaction forming additional hydrogen (Eq. 2). To prevent carbon formation and deposition, sufficient steam is added as a reforming agent. Typically, a steam/methane ratio of two is applied. The resulting equilibrium gas mixture consists of all species, from which the theoretical OCV (OCV_T) can be calculated from the Nernst equation. Deviations from this value would indicate incomplete methane conversion, i.e. a non-equilibrium gas composition.

$$CH_4 + H_2O \leftrightarrow CO + 3H_2 \quad [1]$$

$$CO + H_2O \leftrightarrow CO_2 + H_2 \quad [2]$$

Figure 3 shows iV curves using hydrocarbon containing fuel on Ni/YSZ cells and MSCs at a low temperature of 650 °C. The methane conversion is known to be complete on the Ni/YSZ cell at high temperatures around 850 °C, based on the OCV-value.[30] In this study, the measured OCV (OCV_M) at the Ni/YSZ cell in methane/

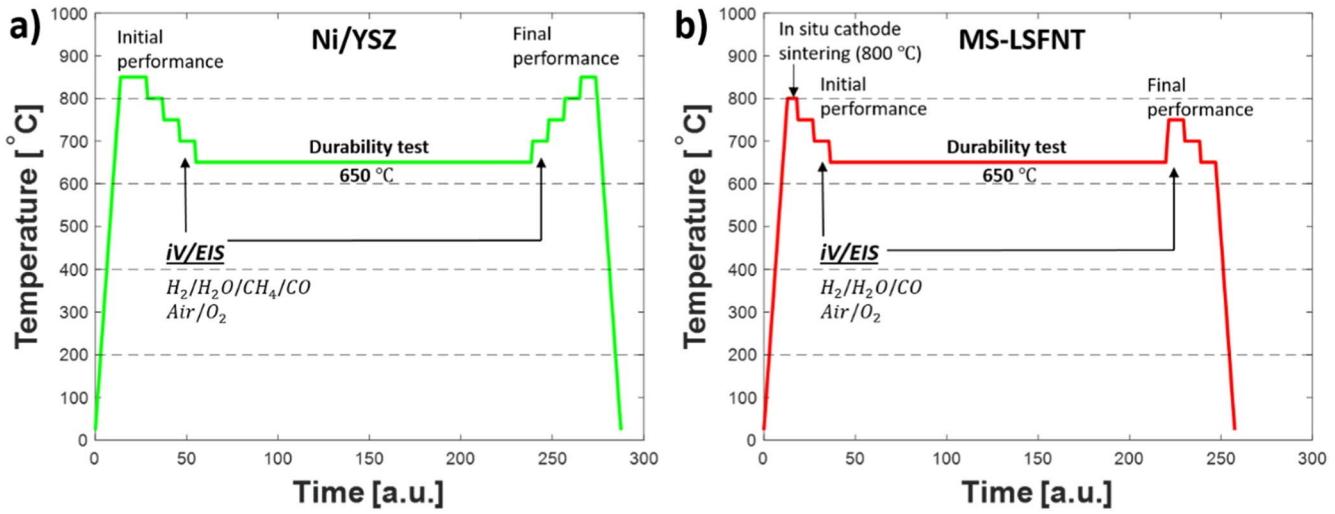

Figure 1. Illustration of full test protocols for the Ni/YSZ cell (a) and the MSCs (b).

Table I. Fingerprint protocol used for the cells. Air and O_2 were used on the cathode side for all conditions.

Cell type	Ni/YSZ	MS-LSFNT
Startup procedure —heating	Heat to 850 °C at 60 °C h^{-1} with N_2 to anode and air to cathode (both 20 l h^{-1})	Heat to 800 °C at 60 °C h^{-1} with H_2/N_2 (1:19) to anode (20 l h^{-1}), air to cathode (40 l h^{-1})
Startup procedure - holding	Change anode gas for NiO-reduction: 2 h H_2/N_2 (1:19), then 1 h in H_2 (both 20 l h^{-1})	5 h hold in pure H_2 to anode, air to cathode (20 l h^{-1} and 140 l h^{-1} respectively), then go to 750 °C
Fingerprint gasses, anode	H_2/H_2O (4, 20, 50%), 25 l h^{-1} CO/ H_2O (1:2), 18 l h^{-1};CO/ H_2O/H_2 (1:1:3), 20 l h^{-1} CH_4/ H_2O (1:2), 18 l h^{-1};	H_2/H_2O (4, 20%), 25 l h^{-1} CO/H_2O (1:2), 18 l h^{-1} CO/ H_2O/H_2 (1:1:3), 20 l h^{-1}
Temperature range	850 °C, 800 °C, 750 °C, 700 °C, 650 °C	750 °C, 700 °C, 650 °C

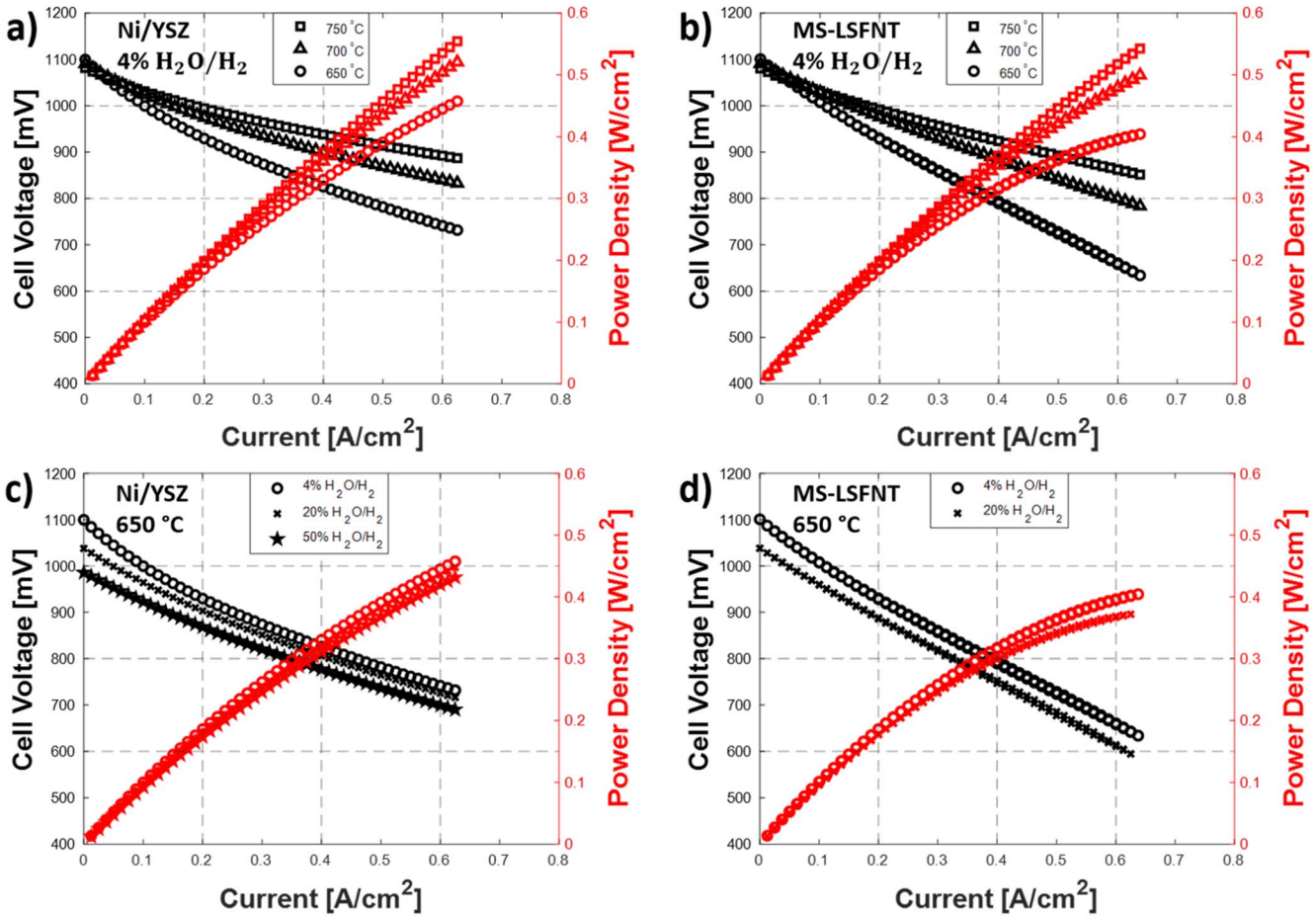

Figure 2. iV curves (black, left axis) and power density curves (red, right axis) in 4% steam/hydrogen at different temperatures for Ni/YSZ (a) and MS-LSFNT (b), and at 650 °C in different steam/hydrogen ratios for Ni/YSZ (c) and MS-LSFNT (d).

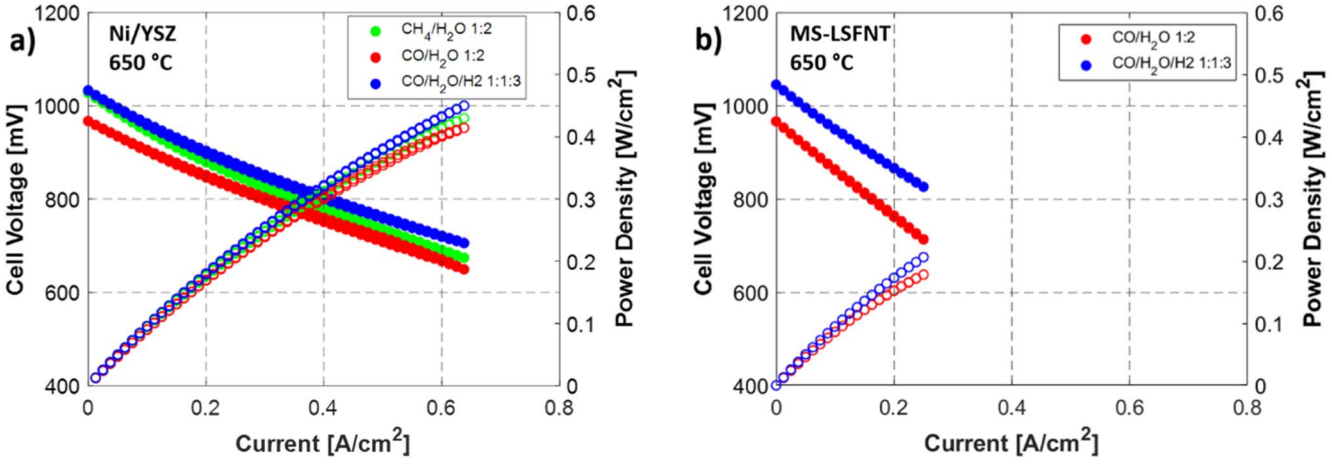

Figure 3. iV curves (full symbol, left axis) and power density curves (open symbols, right axis) at 650 °C in hydrocarbon fuel for Ni/YSZ (a) and MS-LSFNT (b).

steam at 650 °C was 1027 mV, which is only slightly lower (<10 mV) than calculated with the Nernst equation (Table III). Thus, the methane conversion is almost complete at this temperature, with a calculated conversion activity of 86%, based on OCV (Table III).

Methane conversion is known to be much lower on MS-LSFNT cells, where an OCV of 944 mV, corresponding to only 17% conversion at 650 °C, was obtained.[24] This has been assigned to the much lower Ni-content in these electrodes compared to the Ni/YSZ cermet anode. Despite the higher surface area per weight of the infiltrated Ni, this leads to a reduced number of Ni sites available for catalytic conversion of methane. Such a small methane conversion activity does not seem appropriate for industrial applications, where steam reforming is a crucial step if e.g. natural gas is to be used directly. A solution is to use a pre-reformer and feed the obtained reformate gas mixture directly to the SOFC. This would require a certain activity of the fuel electrode for the WGS reaction. To separate the effect of methane reforming (Eq. 1) from the WGS reaction (Eq. 2), CO/H_2O (1:2 ratio) as well as a pre-reformed gas

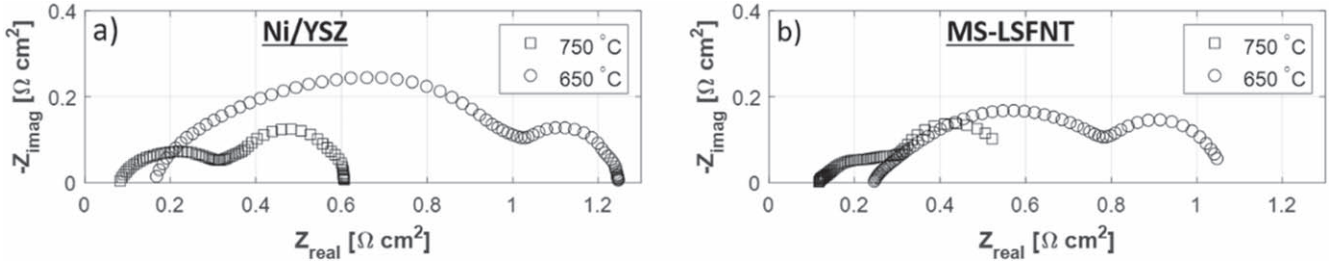

Figure 4. EIS of the Ni/YSZ (a) and MS-LSFNT (b) cells in 4% steam/hydrogen at 750 °C (squares) and 650 °C (circles).

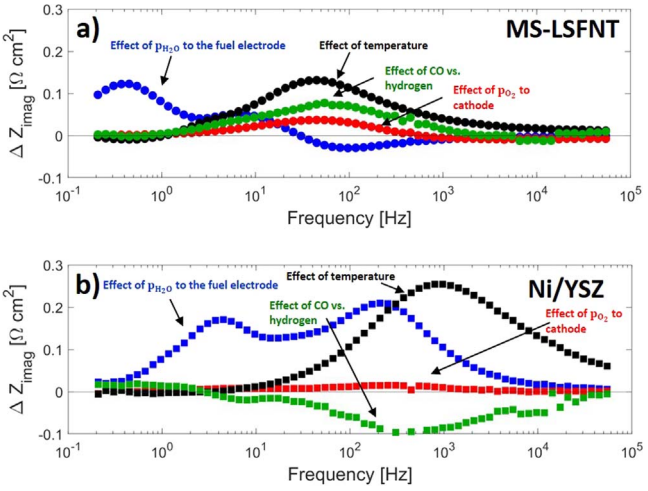

Figure 5. Difference of EIS (bode plots) at OCV for MS-LSFNT (a) and Ni/YSZ (b). Black symbols: 650 °C vs 750 °C with 20% steam/hydrogen. At 650 °C, blue symbols: 4% steam/hydrogen vs 20%, green symbols: CO/steam vs 20% steam/hydrogen, red symbols: air vs oxygen to the cathode.

mixture, corresponding to complete methane conversion (i.e. $CO/H_2O/H_2$ in a 1:1:3 ratio) were fueled directly to both cells. Based on the OCV values at 650 °C (Table III), the equilibrium gas mixture according to the WGS reaction is nearly achieved for both cells. The ASR in CO/H_2O (Table II, grey background) is only 0.49 Ω cm^2 on the Ni/YSZ cell, which is similar to the value in 50% steam/hydrogen. This corresponds well to the equilibrium gas mixture at 650 °C, which—as calculated from thermodynamics—consists of 41% H_2O, 25% H_2, 26% CO_2, 7%–8% CO, and trace amounts of CH_4. Thus, the Ni/YSZ based cell is effective for the WGS reaction at 650 °C. The ASR for the MS-LSFNT cell in CO/H_2O is twice as large (1.04 Ω cm^2) compared to the Ni/YSZ cell, even though the OCV values are comparable. Additionally, the MSC possesses a slightly lower power density (Table II). This points to a lower efficiency of the MS-LSFNT cell in CO containing fuels. This could be caused by lower activity for the WGS reaction, lower activity for direct CO electrochemical oxidation or a combination of both.

Since the cell performances are similar in hydrogen fuel, no difference in electrochemical performance is expected. Additionally, at the present CO/H_2O ratio of 1:2 (i.e. excess steam), the contribution from WGS-reaction should dominate over direct CO electrochemical oxidation. A lower activity for WGS-reaction is surprising considering the comparable OCV values for the two cells. It might be explained by the reduced number of active sites in the MSC, due to the low Ni content compared to SoA. At OCV, there is sufficient catalytic activity for WGS reaction to occur on both cells, whereas the active sites could be occupied for electrochemical oxidation of H_2 (and CO) under current, which could lead to incomplete WGS reaction and larger ASR values. Despite a lower performance than SoA, SOFC-operation in pre-reformed hydrocarbon fuels at low temperature may still be feasible for the MS-LSFNT cell, especially at low-to-moderate current loads.

EIS characterization.—The iV curves recorded during the initial characterization show different performance results for the two cells at different temperatures and fuel gas compositions. The performance of the MSC in terms of ASR was slightly lower than the Ni/YSZ cell, despite the more active electrode materials. In order to reveal more details, EIS was evaluated at OCV-conditions.

Figure 4 shows Nyquist plots in 4% steam/hydrogen for both cells at 750 °C and 650 °C, corresponding to the iV curves in Figs. 2a and 2b. Both resistance contributions (serial (Rs) and polarization (Rp) resistances) increase with decreasing temperature. The polarization resistances are comparable at 750 °C. At 650 °C, the Rp contribution of the Ni/YSZ cell is much larger compared to the MSC. On the other hand, the serial resistance is larger and more temperature dependent for the MSC compared to SoA. Based on the iV curves, where the increase in ASR is larger for the MSC compared to Ni/YSZ as the temperature decreases, the serial resistance is the dominating factor for low temperature performance. Hence, variations in electrolyte material/thickness and electrolyte/

Table II. Summary of ASR [Ω cm^2], power density [W cm^{-2}], and cell voltage [mV] values for the cells around 0.25 A cm^{-2} in hydrogen and C containing fuels

Cell type	Ni/YSZ	MS-LSFNT
750 °C		
{H_2/H_2O (4%)}	0.30 Ω cm^2, 0.24 W cm^{-2} (979 mV)	0.35 Ω cm^2, 0.24 W cm^{-2} (974 mV)
700 °C		
{H_2/H_2O (4%)}	0.40 Ω cm^2, 0.24 W cm^{-2} (954 mV)	0.48 Ω cm^2, 0.24 W cm^{-2} (952 mV)
650 °C		
{H_2/H_2O (4%)}	0.56 Ω cm^2, 0.23 W cm^{-2} (900 mV)	0.72 Ω cm^2, 0.22 W cm^{-2} (892 mV)
{H_2/H_2O (20%)}	0.52 Ω cm^2, 0.22 W cm^{-2} (876 mV)	0.70 Ω cm^2, 0.21 W cm^{-2} (850 mV)
{H_2/H_2O (50%)}	0.48 Ω cm^2, 0.21 W cm^{-2} (843 mV)	—
{CH_4/H_2O (1:2)}	0.55 Ω cm^2, 0.21 W cm^{-2} (850 mV)	—
{CO/H_2O (1:2)}	0.49 Ω cm^2, 0.21 W cm^{-2} (821 mV)	1.04 Ω cm^2, 0.18 W cm^{-2} (713 mV)
{$CO/H_2O/H_2$ (1:1:3)}	0.51 Ω cm^2, 0.22 W cm^{-2} (870 mV)	0.79 Ω cm^2, 0.21 W cm^{-2} (826 mV)

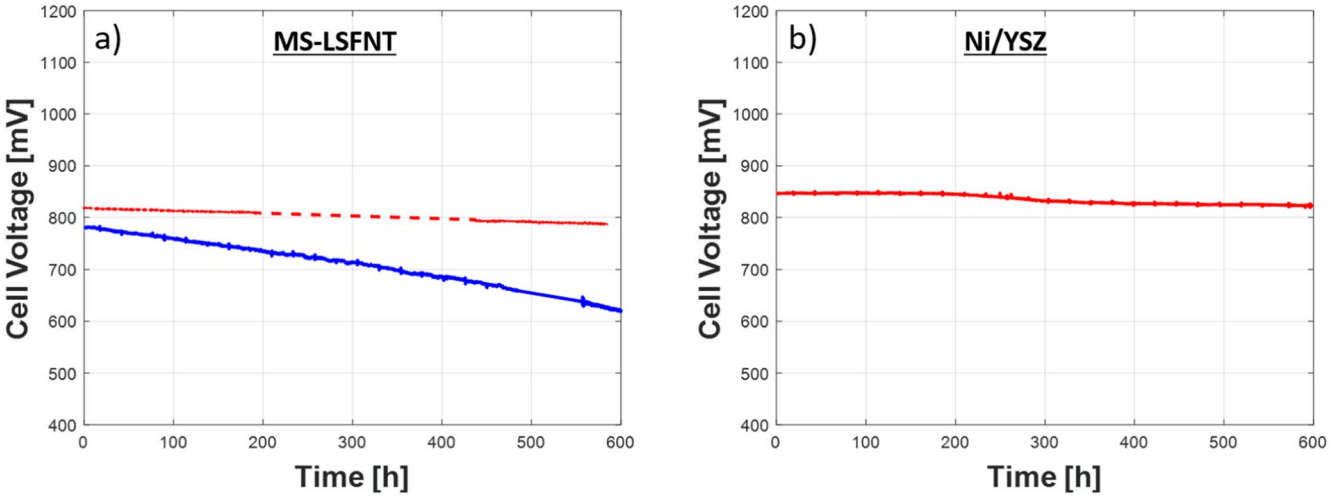

Figure 6. Cell voltage degradation of the cells under current (0.25 A cm^{-2}) at 650 °C for the MSC (a) and the SoA cell (b) in 20% steam/hydrogen(red curves, same raw data for the MSC as used for Ref. 24 in Fig. 9)) and reformate gas, CO/steam/hydrogen (1:1:3) (blue curve).

anode contacting are at least as important as the choice of electrode materials for determining the cell performance.

A way to identify specific electrode processes is to record EIS under different temperatures, fuel-to-anode, and oxygen-partial-pressure-to-cathode compositions, and to observe the changes of EIS. In other words, one condition is changed while keeping all other parameters constant in order to enable the identification of individual anode and cathode contributions to the total impedance of the cell. A simple difference between the spectra (Bode plots) can be used for a rapid visualization of the affected processes. Figure 5 displays the results for both cells, and Table IV illustrates the affected processes under each condition change. The impedance signal associated with the cathode increases for the MSC as the cathode gas changes from oxygen to air. The increase in impedance is between 10-100 Hz. This is in good agreement with earlier observations on LSC and LSC/CGO cathodes.[24,31] Compared to the MSC, the cathode of the Ni/YSZ cell is almost not affected when changing the cathode gas. This might be due to a less active air electrode in the SoA cell, which was not sintered in situ as compared to the cathode in the MSC.

A lower steam/hydrogen ratio results in impedance responses at frequencies of 1-10 Hz and 200 Hz for the Ni/YSZ cell, and at 0.5 Hz, 10 Hz, and 50-100 Hz for MS-LSFNT. The low frequency responses should correspond to gas conversion and diffusion impedance. The signal at 200 Hz (Ni/YSZ) can be attributed to the electrochemical reaction at the triple-phase-boundary (TPB) of the Ni/YSZ electrode. The signal frequency is below typical values reported at higher temperatures (1–4 kHz), which could be a consequence of slower kinetics at lower temperature.[31] The slight decrease around 50-100 Hz for the MSC is caused by reactions in the LSFNT electrode.

A change of fuel gas from 20% steam/hydrogen to CO/steam (1:2) affects the impedance of both cells, but in different ways: the Ni/YSZ cell experiences a lower impedance contribution at and below 1 kHz, whereas the MSC shows an increase around 50-100 Hz. These high frequencies should correspond to fuel electrode processes, not gas conversion and/or gas diffusion. The impedance response for the Ni/YSZ cell can be an effect of a higher steam content in the inlet gas—as mentioned earlier, a complete WGS reaction at 650 °C leads to an equilibrium fuel gas composition of 41% H_2O, 25% H_2, 26% CO_2, and ca. 8% CO. This high steam content results in a lower TPB contribution to the impedance than the 20% steam/hydrogen used as reference in Fig. 5b. The increased impedance contribution for the MSC in CO/steam indicates that the steam content is higher than 20% (i.e. a lower amount of hydrogen available), affecting fuel electrode processes—however, the extent of WGS-reaction cannot be quantified from these plots.

The impedance for the Ni/YSZ cell increases over a broad frequency range from 0.1 to >10 kHz when the temperature is decreased from 750 °C to 650 °C. This indicates an effect of multiple processes within the cell, including ionic transport (i.e. serial resistance, >10 kHz), triple phase boundary reactions in the fuel electrode (around 1 kHz), and cathode impedance (ca. 100 Hz). The MSC shows a significant increase in impedance between 10-100 Hz, where cathode and anode processes overlap (Fig. 5a), and a minor increase at higher frequencies due to increase in ionic transport resistance.

Durability testing in reformate gas.—To assess the durability when using a reformate fuel in low temperature operation of MS-LSFNT, a test was conducted in a relevant fuel composition, corresponding to complete methane conversion (i.e. CO/steam/hydrogen (1:1:3)), over several hundred hours. The parameters

Table III. OCV values [mV] and calculated methane reforming/CO conversion activity [%] at 650 °C.

Cell type	Ni/YSZ	MS-LSFNT
CH_4/H_2O (1:2)		
OCV_T, OCV_M / mV	1034, 1027	1034, 944 (ref. [24])
Reforming activity, CH_4 / %	86	17
Reformed CH_4 ($CO/H_2O/H_2$ (1:1:3))		
OCV_T, OCV_M / mV	1034, 1033	1034, >1034
CO/H_2O (1:2)		
OCV_T, OCV_M / mV	969, 967	969, 966
Conversion activity, CO / %	96	94

Table IV. Impedance response and associated process of the cells when changing conditions.

Fixed conditions Condition change	T = 650 °Fuel gas: 20% H_2O/H_2 Change of cathode gas —from O_2 to air	T = 650 °C Cathode: air Change of H_2O/H_2 ratio—from 20 to 4% H_2O	T = 650 °C Cathode: air Change of anode gas—from 20% H_2O/H_2 to CO/H_2O (1:2)	Cathode: air Fuel gas: 20% H_2O/H_2 Change of temperature from 750 °C to 650 °C
Effect on Ni/YSZ cell impedance	Slight increase in impedance (ca. 100 − 200 Hz)—LSC/CGO cathode response	Increase in impedance at 1 − 10 Hz—due to increased gas conversion and diffusion Increase at ca. 200 Hz—TPB response	Decrease in impedance at and below 1 kHz—TPB response	Increase at and above 10 kHz—ionic transport Increase around 1 kHz—TPB response. Increase at 100 Hz—LSC/CGO cathode response
Effect on MS-LSFNT cell impedance	Increase in impedance (ca. 10 − 100 Hz)—LSC cathode response	Increase in impedance at 0.5 and 10 Hz—due to gas conversion and diffusion, respectively. Decrease around 50 Hz (fuel electrode response)	Increase in impedance around 50 Hz—response from the LSFNT fuel electrode in higher (>20%) steam content,	Increase at and above 10 kHz—ionic transport. Increase from ca. 10 − 100 Hz —overlapping anode and cathode response.

Table V. Summary of degradation rates [% kh^{-1}] at 650 °C and 0.25 A cm^{-2}.

Cell type	Ni/YSZ	LSFNT
20% H_2O/H_2		
FU of 42%	5% kh^{-1}	5% kh^{-1} (Ref. 24)
CH4/H_2O (1:2)		
FU of 48%	–	30% kh^{-1} (Ref. 24)
$CO/H_2O/H_2$ (1:1:3)		
FU of 42%	–	36% kh^{-1} (entire test) and 30% kh^{-1} (first 120 h)

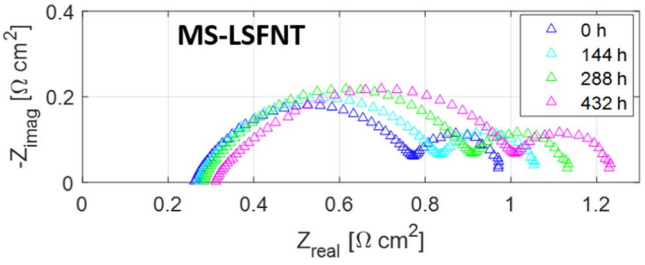

Figure 7. EIS obtained during durability test of the MS-LSFNT cell in reformate fuel gas (CO/steam/hydrogen 1:1:3) at a FU of 42% at 650 °C.

used were similar to a short (120 h) test conducted on MS-LSFNT in an earlier study (650 °C, 0.25 A cm^{-2}, fuel utilization (FU) of 48%) in methane/steam fuel.[24] Due to technical reasons, a FU of 42% was used in this study, as compared to the 48% in the previous study. Degradation rates were calculated as linear degradation rate of cell voltage per 1000 h, and are listed in Table V, together with literature values from previous durability tests on MS-LSFNT cells. Figure 6a displays the cell voltage degradation over time in reformate gas (blue curve) and 20% steam/hydrogen (red curve, same raw data for the MSC as used for Ref. 24 in Fig. 9). The observed degradation rate in reformate fuel gas of 36% kh^{-1} is slightly above the rate reported in methane/steam (30% kh^{-1}). However, considering the initial 120 h, the rates are both 30% kh^{-1} in methane/steam and in the pre-reformed gas mixture, which is six times larger than the reported degradation rate of 5% kh^{-1} in 20 % steam/hydrogen in the earlier study (Fig. 6a, red curve).[24] Hence, the limited methane reforming reaction on the MSC anode is in itself not the only cause of cell degradation. To reveal more details on the degradation process, EIS was evaluated. Nyquist plots obtained during the degradation test on the MS-LSFNT cell are shown in Fig. 7. The increase in serial resistance is minor, which indicates that delamination of layers or oxidation of the steel support is not significant during the durability test. In contrast, the polarization resistance increases significantly over time, specifically the first arc related to electrochemical reactions. For Ni/YSZ cells it is well known that the steam partial pressure in the fuel gas has a significant contribution to the degradation.[32] This is expected to have an influence on the MS-LSFNT cell as well. If the WGS reaction does not proceed to equilibrium, as suggested by the large ASRs in CO containing fuel (Table II), the steam partial pressure will be significantly higher than the apparent fuel utilization would suggest - i.e. the real fuel utilization is significantly higher than 42% if the WGS reaction is incomplete. This could lead to degradation of the LSFNT fuel electrode backbone and/or impacting the infiltrated Ni particles. Another possible degradation mechanism could be carbon deposition, resulting in reduced active sites (Ni) for electrochemical conversion of hydrogen and CO. Neagu et al. reported that exsolved Ni from the B-site of La-doped strontium titanate perovskites is C-tolerant, in contrast to deposited Ni.[33] Hence, carbon deposition on the infiltrated Ni could in principle explain some of the degradation However, we expect C deposition to be suppressed by the chosen gas composition, where steam and CO are both present as 20% of the total gas mixture. Additionally, Ni:CGO infiltrate has been reported to exhibit good C tolerance in CO/CO_2.[34]

SoA-Ni/YSZ in steam/hydrogen.—The Ni/YSZ cell was durability tested in 20% steam/hydrogen (T = 650 °C, current = 0.25 A cm^{-2}, FU: 42%) for benchmarking to MS-LSFNT cells tested previously.[24] Figure 6b displays the cell voltage degradation over time. The degradation rate of 5% kh^{-1} is similar to the known value for MS-LSFNT cells. This indicates that the performance difference under current between MS-LSFNT and Ni/YSZ SoA cells in steam/hydrogen fuel at low temperature (650 °C) is minor. However, the previous test on the MSC included 1000 h of operation at low fuel utilization (10%) prior to testing at a FU of 42%. This might have contributed to some degradation, which is indicated by the lower cell voltage for the MSC at the start of the durability testing at a FU of 42% compared to the Ni/YSZ cell (820 mV and 845 mV, respectively); hence the results are not directly comparable. Nevertheless, it is clear that MS-LSFNT cells have at least similar performance compared to Ni/YSZ cells in steam/hydrogen fuel at low temperature (650 °C) and moderate current load (0.25 A cm^{-2}).

Conclusions

A SoA Ni/YSZ cell and a MSC, with a Ni:CGO infiltrated doped $SrTiO_3$-fuel electrode (LSFNT), were operated in hydrogen and carbon containing fuel, with the aim to compare their performances at different temperatures and fuel gas compositions. Based on the iV curves, the performances in steam/hydrogen are similar at 750 °C, but at 650 °C the MS-LSFNT cell becomes slightly inferior to the Ni/YSZ cell. This is evident in form of significantly higher ASR values for the MSC, although the power densities are similar for the two cells. The corresponding low temperature impedance data showed a lower polarization resistance for the MSC, but a larger serial resistance, the latter associated with the drop in performance found from the iV curves. Hence, a performance superior to SoA could be realized if the serial resistance contribution for the MSC is minimized, e.g. by tailoring the electrolyte and/or anode/electrolyte contacting. Durability testing of the Ni/YSZ cell in 20% steam/hydrogen at 650 °C revealed a degradation rate of 5% kh^{-1}, which is similar to the known value for MS-LSFNT cells. The comparable performance of the MS-LSFNT cells to Ni/YSZ cells in hydrogen fuel, its lower material cost, and mechanical robustness makes it a promising alternative in the aim for lower SOFC operating temperatures.

MS-LSFNT cells are less active for the catalytic reforming of methane with steam than SoA cells. The use of CO/steam (1:2) and a reformate gas mixture corresponding to complete methane conversion (CO/steam/hydrogen (1:1:3)) as fuel gas, respectively, yields OCV values in agreement with the theoretical values calculated from the Nernst equation for both cells. However, the performance of the MSC in CO containing fuels under current reflects that the cell is less effective for the WGS reaction compared to the Ni/YSZ based cell. This is probably caused by the low Ni content in the LSFNT electrodes, leading to incomplete WGS reaction when the catalytic sites are occupied by electrochemical oxidation of hydrogen and CO.

The degradation rate of 30% kh^{-1} obtained from the durability test in the ideal methane reformate gas mixture is similar to the value found in an earlier study on MS-LSFNT cells in methane/steam. Hence, cell degradation is not only caused by the limited methane reforming reaction itself on the LSFNT-fuel electrode. It could be caused by high steam content, due to incomplete WGS reaction, leading to degradation of the LSFNT fuel electrode backbone and/or impacting the infiltrated Ni particles. C-deposition is not expected in the utilized gas mixtures. The degradation rate for the MS-LSFNT cell in both methane/steam and the pre-reformed gas mixture is 6 times larger than those reported in hydrogen/steam fuel, at similar FU, current density and temperature. Hence, further tailoring of electrode composition and microstructure is required to minimize cell degradation in carbon containing fuels.

Acknowledgments

This project has received funding from the Fuel Cells and Hydrogen 2 Joint Undertaking (JU) under grant agreement No 874577, EU NewSOC. The JU receives support from the European Union's Horizon 2020 research and innovation programme and Denmark, France, Italy, Spain, Poland, Netherlands, Greece, Finland, Estonia, Germany, United Kingdom, Switzerland. We are grateful to L. Knudsen and K. Brodersen for cell manufacture, H. Henriksen, F. Capotondo, and A. Erdogan for technical assistance and contribution to cell testing.

ORCID

J. O. Christensen https://orcid.org/0000-0003-3502-7927
B. R. Sudireddy https://orcid.org/0000-0003-0981-445X
A. Hagen https://orcid.org/0000-0003-2001-8040

References

1. S. A. Saadabadi, A. T. Thattai, L. Fan, R. E. F. Lindeboom, H. Spanjers, and P. V. Aravind, *Renew. Energ.*, **134**, 194 (2019).
2. J. Meusinger, E. Riensche, and U. Stimming, *J. Power Sources*, **71**, 315 (1998).
3. (https://solidpower.com/en/bluegen). Accessed: 2021-03-26.
4. (https://adelan.co.uk/). Accessed: 2022-02-18.
5. (https://bloomenergy.com/technology/). Accessed: 2022-04-06.
6. I. Alstrup, M. T. Tavares, C. A. Bernardo, O. Sørensen, and J. R. Rostrup-Nielsen, *Mat.Corros.*, **49**, 367 (1998).
7. Y. Matsuzaki and I. Yasuda, *Solid State Ionics*, **132**, 261 (2000).
8. A. Hagen, G. B. Johnson, and P. Hjalmarsson, *J. Power Sources*, **272**, 776 (2014).
9. M. C. Verbraeken, T. Ramos, K. Agersted, Q. Ma, C. D. Savaniu, B. R. Sudireddy, J. T. S. Irvine, P. Holtappels, and F. Tietz, *Rsc Adv.*, **5**, 1168 (2015).
10. M. C. Verbraeken, B. Iwanschitz, A. Mai, and J. T. S. Irvine, *J. Electrochem. Soc.*, **159**, F757 (2012).
11. B. R. Sudireddy et al., *Fuel Cells*, **17**, 508 (2017).
12. B. D. Madsen, W. Kobsiriphat, Y. Wang, L. D. Marks, and S. A. Barnett, *ECS trans.*, **7**, 1339 (2007).
13. D. Neagu, G. Tsekouras, D. N. Miller, H. Ménard, and J. T. S. Irvine, *Nat. Chem.*, **5**, 916 (2013).
14. T. Jardiel, M. T. Caldes, F. Moser, J. Hamon, G. Gauthier, and O. Joubert, *Solid State Ion.*, **181**, 894 (2010).
15. V. V. Krishnan, *WIREs Energy Environ.*, **6**, e246 (2017).
16. M. Dewa, W. Yu, N. Dale, A. M. Hussain, M. G. Norton, and S. Ha, *Int. J. Hydrog*, **46**, 33523 (2021).
17. M. C. Tucker, *J. Power Sources*, **195**, 4570 (2010).
18. M. Haydn, C. Bischof, D. Udomsilp, A. K. Opitz, G. Bimashofer, W. Schafbauer, M. Brandner, and M. Bram, *ECS trans.*, **78**, 1993 (2017).
19. D. Udomsilp et al., *Cell Rep. Phys. Science*, **1**, 100072 (2020).
20. M. M. Welander, B. Hu, and M. C. Tucker, *Int. J. Hydrog*, **47**, 11261 (2022).
21. M. Brandner, M. Bram, J. Froitzheim, H. P. Buchkremer, and D. Stoever, *Solid State Ionics*, **179**, 1501 (2008).
22. P. Blennow, J. Hjelm, T. Klemensø, Å. H. Persson, S. Ramousse, and M. Mogensen, *Fuel Cells*, **11**, 661 (2011).
23. F. Shen, R. Wang, and M. C. Tucker, *J. Power Sources*, **474**, 228618 (2020).
24. A. Hagen, X. Sun, B. R. Sudireddy, and Å. H. Persson, *J. Electrochem. Soc.*, **167**, 104510 (2020).
25. J. Nielsen, Å. H. Persson, B. R. Sudireddy, J. T. S. Irvine, and K. Thydén, *J. Power Sources*, **372**, 99 (2017).
26. J. Nielsen, T. Klemensø, and P. Blennow, *J. Power Sources*, **219**, 305 (2012).
27. T. Klemensø, J. Nielsen, P. Blennow, Å. H. Persson, T. Stegk, B. H. Christensen, and S. Sønderby, *J. Power Sources*, **196**, 9459 (2011).
28. P. H. Larsen and K. Brodersen, (2008), (US2008124602-A1; JP2008130568-A; EP1930974-A1; CN101242003-A; CA2611362-A1; KR2008047282-A; KR966845-B1).
29. J. Hjelm, M. Søgård, R. Knibbe, A. Hagen, and M. Mogensen, *ECS trans*, **13**, 285 (2008).
30. A. Hagen, H. Langnickel, and X. Sun, *Int. J. Hydrog*, **44**, 18382 (2019).
31. A. Hauch, K. Brodersen, M. Chen, and M. B. Mogensen, *Solid State Ion*, **293**, 27 (2016).
32. A. Ploner, A. Hagen, and A. Hauch, *Fuel Cells*, **17**, 498 (2017).
33. D. Neagu, T. Oh, D. N. Miller, H. Ménard, S. M. Bukhari, S. R. Gamble, R. J. Gorte, J. M. Vohs, and J. T. S. Irvine, *Nat. Commun*, **6**, 8120 (2015).
34. T. L. Skafte, B. R. Sudireddy, P. Blennow, and C. Graves, *ECS trans*, **72**, 201 (2016).